Journal of Biomedical Optics 7(3), 388–397 (July 2002)

Fiber optic probe for polarized reflectance spectroscopy *in vivo*: Design and performance

Alexey Myakov
Linda Nieman
Lorenz Wicky
Urs Utzinger
Rebecca Richards-Kortum
Konstantin Sokolov
University of Texas
Biomedical Engineering Program
Austin, Texas 78712

Abstract. We present the design and construction of a fiber optic probe for elastic light scattering spectroscopy *in vivo* with polarized excitation and polarization sensitive detection. The performance of the fiber probe is evaluated using a suspension of polystyrene spheres placed atop a diffusely scattering substrate, and it demonstrates that the size-dependent characteristics of the scatterers can be extracted in the presence of a highly diffusely scattering background using a linear combination of forward and backward Mie scattering components of the scatterers. Subsequently, Mie theory calculations are performed over a broad range of diagnostically relevant parameters of nuclei—mean diameter, size distribution, and relative refractive index—to understand how the polarized reflectance measurements with the fiber probe can be used to extract morphological information about epithelial tissue. Finally, the feasibility of *in vivo* measurements with the fiber optic based polarization sensitive light scattering spectroscopy is demonstrated. © *2002 Society of Photo-Optical Instrumentation Engineers.*
[DOI: 10.1117/1.1483314]

Keywords: elastic light scattering; polarized light; reflectance spectroscopy; cancer diagnosis.

Paper JBO TP-04 received July 6, 2001; revised manuscript received Mar. 1, 2002; accepted for publication Mar. 19, 2002.

1 Introduction

An estimated 1,268,000 new cases of cancer will be diagnosed in the United States in the year 2001 and of those an estimated 553,400 Americans will die from cancer.[1] Cancer is the second leading cause of death in the U.S. exceeded only by heart disease. The majority of cancers are of epithelial origin. Most epithelial cancers are preceded by a curable precancerous stage.[2] Therefore, early diagnosis of pre-invasive epithelial neoplasia can potentially reduce both the incidence and mortality associated with cancer.

A number of screening and detection tools have been developed to improve detection of pre-cancers; most of these are based on the qualitative analysis of the interaction of light with tissue, including the pap smear, colonoscopy, and colposcopy for example. However, the sensitivity and specificity of most clinically available screening and detection techniques are limited. A number of new quantitative optical techniques for improved cancer detection have been introduced and tested *in vitro* and *in vivo* recently. Many of these show promise of increasing both the sensitivity and specificity.[3–5] One particularly promising technique relies on the quantitative analysis of polarized light which is elastically scattered by epithelial tissue;[6–9] the intensity versus wavelength dependence of this scattering may be related to changes in nuclear size, density, and chromatin texture.

Pre-cancerous lesions are characterized by increased nuclear size, increased nuclear/cytoplasmic ratio, hyperchromasia and pleomorphism.[2] Elastic light scattering spectroscopy may provide a tool with which to assess tissue morphometry by recovering the typical scatterers' sizes and their refractive indices, both encoded in the wavelength dependence of scattering. Mourant et al. showed that multiwavelength elastic scattering measurements are sensitive to morphological features such as the scatterer size and refractive index,[10] and that Mie theory could be used to estimate the scattering particle size of intralipid phantoms from elastic scattering spectra. Later Perelman et al.[7] observed a fine periodic structure in the wavelength in light backscattered from mucosal tissue. In these experiments, tissue was illuminated with unpolarized light and reflectance spectra were measured. The multiple scattering background that masks the periodic component was modeled numerically and subtracted from measured spectra to extract the periodic component. They attributed this oscillatory component to single scattering from surface epithelial cell nuclei. By analyzing the amplitude and frequency of the fine structure, the density and size distributions of these nuclei were extracted. Obviously, the accuracy of this approach depends on the capability of the physical model to account for multiple scattering and absorption of the stroma. Backman et al.[8] and Sokolov et al.[6] later showed that the large diffusive background and strong hemoglobin absorption could be significantly reduced by illuminating tissue with polarized light and detecting the elastic scattered light at the parallel and perpendicular polarizations. Backman et al. reported results from phantoms, including polystyrene beads and normal and malignant cells, and they indicated that polarized elastic light scattering spectroscopy is a promising tool that can potentially provide a quantitative estimate of the size distributions of cell nuclei. Moreover, it can provide addi-

Address all correspondence to Konstantin Sokolov. Tel: 512-471-7440; Fax: 512-475-8854, E-mail: kostia@mail.utexas.edu

1083-3668/2002/$15.00 © 2002 SPIE

tional information about the relative refractive index of the nucleus.

Sokolov et al.[6] reported results of the first *in vivo* study using a tabletop setup to measure polarized elastic scattering spectra. The method was first tested on a number of phantoms modeling epithelial tissue and on cervical biopsies. Then *in vivo* reflectance spectra of the oral cavity were measured and sizes of the nuclei were quantified. While these measurements were made *in vivo*, the optical setup did not allow easy access to mucosal surfaces because it used macroscopic optical components. Further advances in instrumentation are required to enable larger clinical trials with easier access to mucosal surfaces.

One potential approach to enable clinical measurements is to rely on polarization sensitive optical imaging. This approach has already been demonstrated on skin,[11–13] and could be successfully utilized to enhance singly scattered light. However, upgrading polarization imaging to provide the wavelength dependent information necessary to extract the nuclear sizes could significantly increase the cost.

There are several important issues, which must be addressed in order to advance polarized elastic light scattering spectroscopy to use in clinical practice. An important practical issue is to develop fiber optic probes that enable minimally invasive access to the many internal organs covered with epithelial tissue such as the oral cavity, larynx, cervix, esophagus, stomach, colon, bladder, and lung. In this paper we present the design and construction of a fiber optic probe for elastic polarization sensitive spectroscopy which can be applied for clinical studies. Using a suspension of polystyrene beads we demonstrate that the fiber probe can be used to extract the size-dependent characteristics of scatterers in the presence of a highly diffusely scattering background. We show that reflectance spectra collected with the fiber probe can be described as a linear combination of forward and backscattering components of the scatterers which can be derived from Mie theory calculations. We perform Mie theory simulations over a broad range of important morphological parameters—the mean nuclear diameter, nuclear size distribution, and nuclear relative refractive index—to evaluate the sensitivity of polarized reflectance spectroscopy with the fiber probe to morphology of epithelial tissue. Finally, we demonstrate the capability of polarization sensitive light scattering spectroscopy to estimate directly the sizes and size distributions of nuclei in oral cavity mucosa *in vivo*.

2 Methods

2.1 Fiber Probe Construction

Figure 1 illustrates the design concept of our optical fiber probe for polarized reflectance measurements *in vivo*. The probe consists of a fiber that delivers polarized illumination to the tissue site of interest and two independent fibers for simultaneous collection of components of tissue scattering with polarizations parallel and perpendicular to the incident light. The collection fibers are located symmetrically relative to the excitation fiber. There are two major considerations which must be taken into account when designing and building the probe. First, the distance between the illumination and collection fibers should be small to minimize collection of multiply scattered light and to maximize collection of light singly scattered in the epithelial layer.[14] Second, the fiber's numerical aperture (NA) and separation must be adjusted appropriately to avoid collection of Fresnel reflections from the window surface and the tissue surface. We can control the distance between the optical fibers, their numerical apertures, and the thickness of the optical window. These parameters were adjusted to optimize the design of the optical probe to satisfy both requirements.

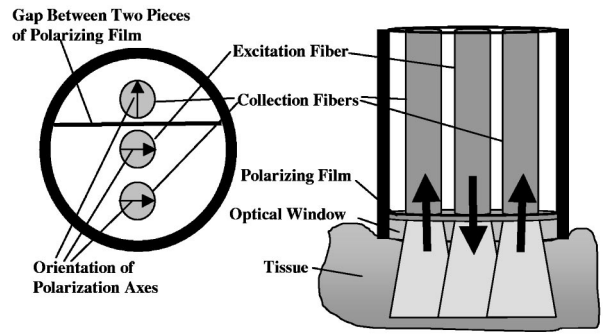

Fig. 1 Schematic of the probe design for polarized reflectance measurements.

The precise geometry of the fiber probe constructed and tested here is shown in Figure 2. The probe was built using three 200 micron core diameter fibers with 0.22 NA. The edge-to-edge separation between fibers was 100 μm. To achieve the separation and to position the fibers symmetrically relative to each other, the fibers were first positioned and glued inside a stainless steel disk [Figure 3(a)]. The disk, with a diameter of $\sim$3.4 mm and thickness of $\sim$1.52 mm, has three holes approximately 254 μm in diameter to accommodate optical fibers. The holes were made by laser drilling (LAI Companies). After the disk and fibers were polished, two pieces of polarization film (Polaroid Corp.) with polarization axes perpendicular to each other were positioned and glued on the disk surface using an optically transparent, biocompatible glue (Epotek 301-2, Epoxy Technology) [Figures 3(b) and 3(c)]. The glue was also used to place a fused silica protective optical window on the top of the fiber probe. Finally, the disk assembly was placed inside a stainless steel tube and the gap

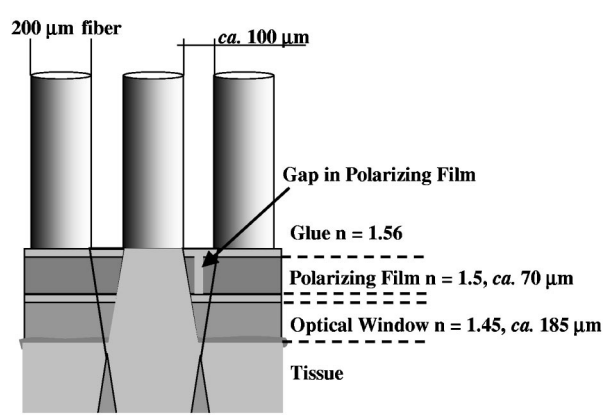

Fig. 2 Geometry of the fiber probe for polarized reflectance measurements.

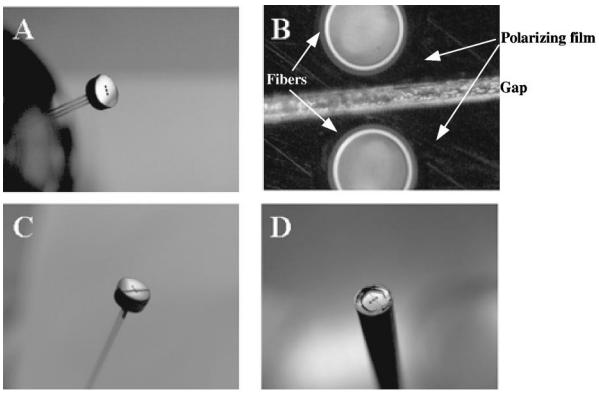

Fig. 3 Major steps in manufacturing the fiber probe: (a) mounting illumination and collection optical fibers in a fiber disk; (b) gluing the polarizing films; (c) a photograph obtained using a light microscope showing a gap between two pieces of polarizing film positioned in front of optical fibers; (d) gluing a fused silica protective optical window on top of polarizing films, placing the disk assembly inside a stainless steel tube, and sealing the gap between the tube and the disk assembly with a biocompatible glue.

between the tube and the disk was filled using the epoxy glue [Figure 3(d)].

The illumination fiber was connected to a Xe pulsed lamp (Hamamatsu, L7685) which provides $\sim 4\ \mu$s pulses with 30–60 Hz repetition rate. The scattered light collected was focused onto the 250 μm entrance slit of a single grating spectrograph (f/3.8, 300 lines/mm grating, Monospec 18, Jarrel Ash) coupled to a gated intensified photodiode array detector (IRY-700, Princeton Instruments). The detector was set to gated mode and was open only for the duration of a pulse from the Xe lamp. Delay times were controlled by a pulse generator. The use of the pulsed lamp and the gated detector allowed all measurements to be performed under room light illumination. This was important in order to reduce the patient's anxiety and to make operation of the device more convenient for clinical practitioners. A PC computer controlled data acquisition. A mercury lamp (ORIEL) was used for wavelength calibration of the spectrometer.

2.2 Samples

Polystyrene beads (5 μm diameter) were purchased from Bangs Laboratories. Suspension cultures of human oral cavity epithelial cells (line 1483) were provided by the University of Texas M. D. Anderson Cancer Center.

Suspensions of 5 μm beads in water were placed atop a diffusely scattering substrate (SRS-99, Labsphere). The substrate strongly depolarizes the excitation polarization and mimics the multiple scattering produced in the stromal layer of epithelial tissue. The concentration of 5 μm polystyrene beads was chosen so that the beads would approximately form a monolayer if they all settled down on the surface of the substrate. To prevent the beads from aggregating, 3 mg/mL of bovine serum albumin (BSA) was added to the water solution.

Next, epithelial cells were used in place of polystyrene beads. As described in our earlier work[6] we used a high concentration of bovine serum albumin to match the refractive index of the cytoplasm with the refractive index of the surrounding medium. This effectively eliminates the cytoplasm as an optical interface and allows the scattering of nuclei to be directly assessed. The concentration of BSA that provides the refractive index matching between the cytoplasm and the surrounding medium was determined using phase-contrast microscopy. The BSA concentration was adjusted until the visible phase-contrast mismatch between the surrounding medium and the cellular cytoplasm was eliminated.[6] The 1483 oral epithelial cell line was used for these experiments. The cells were received in a culture medium and were first washed three times in PBS buffer. Then they were resuspended in 20% (g/100 mL) BSA in PBS. The cells were placed on top of the diffusively scattering substrate at a concentration which corresponded to about 10–15 monolayers.[6] The cells were structurally sound after the optical measurements as evaluated under the light microscope.

Spectral properties of the stroma were measured using two different biological models: a stromal portion of cervical biopsies and collagen gels. Collagen gels were prepared in the manner described in Ref. 15. Cervical biopsies were obtained from the Cooperative Human Tissue Network (CHTN). Three samples of cervical biopsy were measured. Both models yield similar scattering properties of stroma which were used in fitting the polarized reflectance spectra collected *in vivo*. The structure of cervical squamous epithelium is similar in structure to oral squamous epithelium. Therefore cervical biopsies were used to model properties of squamous epithelium of oral cavity.

Normal volunteers were recruited at the University of Texas at Austin for *in vivo* reflectance measurements of the oral cavity mucosa. Informed consent was obtained and the study was reviewed and approved by the Internal Review Board of the University of Texas at Austin.

3 Data Analysis

For each sample, elastically scattered light was measured with polarization parallel and perpendicular to the polarization of the illumination light. Dark current was recorded and subtracted from all measured spectra. The following depolarization ratio (D) was calculated:

$$D(\lambda)=\frac{I_{\parallel}(\lambda)-I_{\perp}(\lambda)}{I_{\parallel}^{S}(\lambda)+I_{\perp}^{S}(\lambda)}, \tag{1}$$

where $I_{\parallel}(\lambda)$ is the component of the light scattered by the sample with polarization parallel to the incident light, $I_{\perp}(\lambda)$ is the component with polarization perpendicular to the incident light, and λ is the wavelength of the incident light. The normalization term in the denominator is the total intensity of light (the perpendicular plus the parallel components) collected from a diffuse scattering substrate alone. The normalization accounts for the spectral characteristics of the excitation lamp and the spectrometer. The ratio $D(\lambda)$ is called the depolarization ratio throughout this paper.

3.1 Theoretical Model for Spectra Collected with the Fiber Probe

To understand depolarization ratio spectra obtained with the fiber optic probe we used the approach described in Ref. 6 for a benchtop polarized reflectance spectrometer. Our theoretical analysis revealed that the depolarization ratio spectra can be

described using a linear combination of forward scattering, backward scattering, and the depolarization ratio for stroma. The final expression for the depolarization ratio is given by

$$D(\lambda)=\frac{I_{\parallel}(\lambda)-I_{\perp}(\lambda)}{I_{\parallel}^{S}(\lambda)+I_{\perp}^{S}(\lambda)}$$
$$=a(\rho)B(\lambda)+b(\rho)S(\lambda)F(\lambda)+S(\lambda),$$
$$F(\lambda)=\int_{\theta_F}p(\theta,\lambda,\overline{d},\Delta d)\sin\theta d\theta,$$
$$B(\lambda)=\int_{\theta_D}p(\theta,\lambda,\overline{d},\Delta d)\sin\theta d\theta, \tag{2}$$
$$p(\theta,\lambda,\overline{d},\Delta d)=\langle p(\theta,\lambda,d)\rangle_{N(d)}=\int_0^{\infty}p(\theta,\lambda,d)N(d)dd,$$

where d is the nuclear diameter, $p(\theta,\lambda,\overline{d},\Delta d)$ is the scattering phase function averaged over the distribution of nuclear diameters $N(d)$, $\overline{d}$ is the average nuclear diameter, Δd is the corresponding standard deviation, ρ is the density of nuclei (number of nuclei per unit volume), θ is the angle between the detection and illumination angles, θ_D is the range of backward scattering angles, θ_F is the range of forward scattering angles, $a(\rho)$ and $b(\rho)$ are parameters that depend on the density of nuclei (ρ), and $S(\lambda)$ is the depolarization ratio profile of stroma. $S(\lambda)$ was determined in experiments on epithelial biopsies described Sec. 2.2. Note that the distribution of nuclear diameters and of wavelength dependence of scattering is encoded in the term $p(\theta,\lambda,\overline{d},\Delta d)$, which can be calculated using Mie theory if the nuclei are assumed to be homogeneous spheres.

The proposed model is based on the assumptions that, one, the epithelium is optically thin and, therefore, the reflectance signal that originates from the epithelium is determined primarily by single scattering events. Second, the polarization state is not changed by a single scattering event. Third, the incident light is effectively depolarized by the stroma, and only a small fraction retains its original polarization. Fourth, the actual and relative refractive indices of scatterers and medium are both nondispersive.

The typical thickness of squamous epithelium is on the order of 150–300 μm and the scattering coefficient varies from 110 cm^{-1} for 400 nm to 70 cm^{-1} for 600 nm.[16] Therefore, the typical number of scattering events photons undergo before reaching stroma is approximately 1–2. Thus, the single scattering approximation is applicable in this case.

Since polarization can potentially be altered as a result of a single scattering event we performed numerical modeling of the polarization ratio intensities for two different scattering particles in our probe geometry. The refractive indices of the medium and particles were assumed to be $n_{\text{med}}=1.374$ and $n_{\text{par}}=1.4235$, respectively. Figures 4(a) and 4(b) show a comparison of the polarization ratio intensity plots for a Rayleigh scatterer (diameter $D=0.06$ μm) and a typical nucleus ($D=6$ μm). The black corresponds to the conservation of the original polarization after a single scattering event. The white corresponds to a scattering event with changes in the polarization of light. The definitions of scattering angles φ and θ and of the polarization ratio are described in detail in Ref. 17. Our probe collects scattering events with $\varphi\in(-9°;9°)$, $\theta_F\in(0°;9°)$, and $\theta_B\in(162°;171°)$. Although scattering at some angles can alter the original state of polarization, the changes in polarization after a single scattering do not exceed 5% for our probe geometry [Figures 4(c) and 4(d)]. Therefore, our assumption that the polarization state is preserved after a single scattering event is valid.

4 Implementation of the Model

The experimental depolarization ratio spectra obtained *in vivo* were fit to a linear combination of forward and backward scattering terms and a stromal depolarization ratio profile $S(\lambda)$ [Eq. (2)]. The relative mean diameter was varied within physiologically reasonable limits. A standard deviation (Δ) of nuclear size distribution $\Delta=0.6$ μm was previously reported in morphometric studies of normal oral epithelium of the cheek.[18] We used this value to simplify the Mie theory calculations. It was assumed that scatterers were homogeneous and nondispersive spheres, hence, we were able to utilize Mie theory. The phase function, $p(\theta,\lambda,d)$, was calculated from Mie theory and was averaged for each wavelength over a Gaussian distribution of nuclear diameters $N(d)$ with center $\overline{d}$ and standard deviation Δd. The forward and backward components were computed using Mie theory by integrating the phase function over the following ranges of angles $\theta_F\in(0°;9°)$ and $\theta_B\in(162°;171°)$, which were calculated with respect to the delivery/acceptance angles of fibers in tissue and the geometry of the probe. A linear non-negative least squares algorithm was used to obtain a fit for each set of nuclear morphometric parameters. Then the standard sum of the squared error (SSE) between the experimental spectrum and the fit obtained was determined. The best fit was the one with the smallest value of the SSE. The Mie code and the fitting were both implemented using MATLAB to provide additional flexibility over commercially available Mie software. The MATLAB code was verified by comparing its results to tabulated scattering curves published by van de Hulst.[17]

5 Results

To determine whether the collection fibers collect light with polarization parallel and perpendicular to the polarization of the illumination light according to the probe design, the fiber probe was placed in direct contact with a mirror and the illumination fiber was connected to a continuous wave (cw) light source. Then signals were monitored in both collection fibers as the mirror was moved away from the probe using a calibrated microtranslation stage. No signal in either collection fiber was observed when the probe was in direct contact with the mirror and a strong signal was detected in the fiber which collects light with polarization parallel to that of the illumination light when the mirror was moved more than ~ 20 μm from the probe. Practically no signal (~ -30 dB compared to the fiber collecting parallel polarization) was detected through the fiber collecting light with polarization perpendicular to that of illumination light at any separations between the mirror and the probe. In a separate experiment, we compared the collection efficiency of both collection fibers by illuminating the distal end of the probe with a nonpolarized light source.

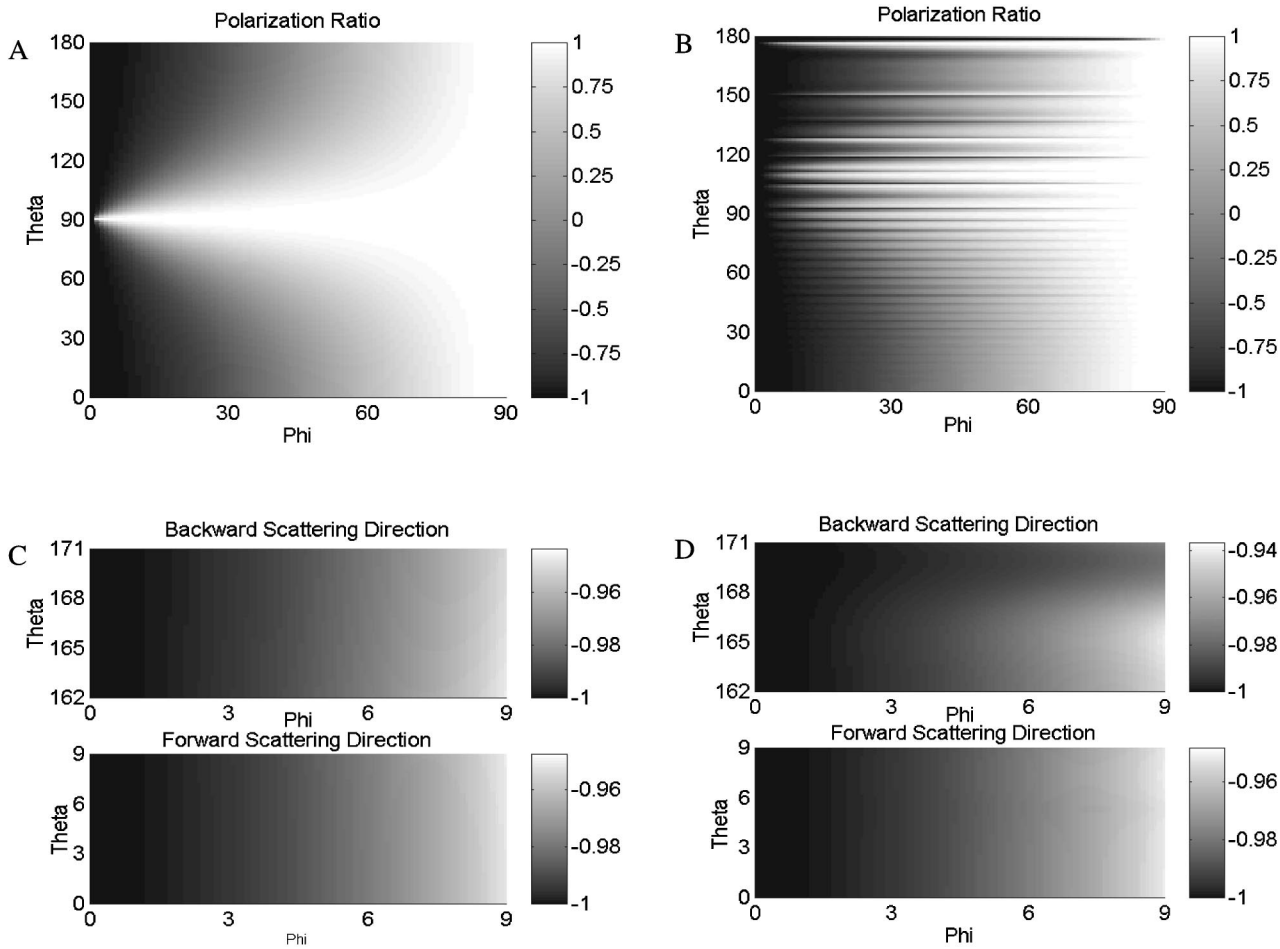

Fig. 4 Calculated polarization ratio plots for two particles with refractive index of $n_{par}=1.4235$ in a medium with refractive index of $n_{med}=1.374$ and incident wavelength of $\lambda=600$ nm: (a) polarization plot for a Rayleigh scatterer with diameter of 0.06 μm for the entire range of scattering angles φ and θ; (b) polarization plot for a nucleus-like scatterer with diameter of 6 μm for the entire range of scattering angles φ and θ; (c) polarization plot for a Rayleigh scatterer with diameter of 0.06 μm for the ranges of scattering angles φ and θ sampled with our probe; (d) polarization plot for a nucleus-like scatterer with diameter of 6 μm for the ranges of scattering angles φ and θ sampled with our probe.

The amount of light collected by both fibers was the same within 4%–5%. These results show that the two pieces of polarizing film positioned in front of the two collection fibers and the illumination fiber are indeed oriented perpendicular relative to each other as shown in Figure 2. The experiment with the mirror also showed that simple Fresnel reflections are collected only for surfaces more than ~ 20 μm distant from the tip of the probe. So, Fresnel reflections from the tissue surface can be totally avoided if the probe is placed at a site in direct contact with a tissue of interest.

After evaluation of the probe geometry we determined whether the probe could be used to detect the size dependant signatures of scatterers in the presence of a diffusely scattering background. We used a suspension of polystyrene beads ($n=1.59$) with a diameter of 5 μm in water ($n=1.33$) placed atop a highly diffusely scattering substrate whose spectral reflection profile is sufficiently flat and can be approximated by a constant dc offset. The concentration of the beads was chosen so that the beads would form a monolayer if they all settled down on the surface. Figure 5 shows that the experimental depolarization ratio spectrum obtained for the beads can be described by using a linear combination of forward and backward scattering components derived from Mie theory as predicted by our model.

We demonstrated previously that polarized reflectance spectra of epithelial tissue can be accounted for by scattering characteristics of nuclei.[6] However, to study the morphology of epithelial tissue *in vivo* using polarized reflectance spectroscopy it is important to understand how changes in nuclear morphology, which include the average diameter, standard deviation, and refractive index of nuclei, can affect both the forward and backward scattering components of tissue. To investigate this dependence, we performed Mie theory calculations over a broad range of morphological parameters. The results are summarized in Figure 6. The mean diameter ranged from 4 to 8 μm with a fixed standard deviation of 0.5 μm and relative refractive index of nuclei $n_{nucl}=1.036$.

Figures 6(a) and 6(b) show the changes in the spectra of forward and backward scattering as the mean nuclear diameter is varied. The changes of forward and backward scattering spectra corresponding to alterations in the width of the nuclear distribution, ranging from 0.1 to 1.7 μm with constant mean diameter (4.7 μm) and relative refractive index (n_{nucl}

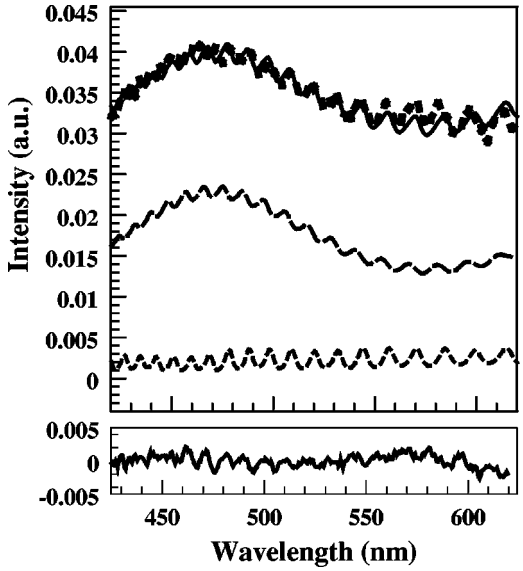

Fig. 5 5 μm polystyrene beads in water: Experimental depolarization ratio reflectance spectrum (dotted curve), forward (long dashed curve) and backward (short dashed curve) scattering components, and theoretical fit (solid curve) obtained from Mie theory calculations. The inset at the bottom shows a differential spectrum between the experimental and the fitting curves.

$=1.036$), are depicted in Figures 6(c) and 6(d), respectively. The curves shown in Figures 6(e) and 6(f) summarize the changes in the scattering components associated with changes in relative refractive index ranging from 1.03 to 1.048, while the mean diameter and standard deviation of nuclear sizes remained constant, at 4.7 and 0.5 μm, respectively.

To quantitatively characterize changes in the *amplitude* of these different curves we calculated the relative amplitude (I_{rel}) of each curve, which is defined as the ratio of the maximum intensity value (I_{max}) minus minimum intensity value (I_{min}) divided by the average intensity value of the spectrum:

$$I_{\mathrm{rel}}=\frac{I_{\mathrm{max}}-I_{\mathrm{min}}}{1/2(I_{\mathrm{max}}+I_{\mathrm{min}})}.$$

As can be seen, both the forward and the backscattering spectra [Figures 6(a) and 6(b)] undergo distinct changes with changes in the mean scatterer diameter. However, the relative amplitude changes of the forward component vary 50% as the mean diameter increases from 4 to 8 μm, whereas the relative amplitude changes in the backward component vary by 0.5% up to 4%. Because the relative changes in the shape of the backscattering spectra are much smaller as the mean nuclear diameter is changed, this component is less sensitive to changes in this morphological parameter.

The dependences of forward and backscattering spectra on the width of the size of the nuclear distributions are shown on the same relative scale in Figures 6(c) and 6(d), respectively. The backscattering component shows a strong dependence on the width of the size distribution for narrow distribution changes from 0.1 to $\sim$0.3 μm but becomes relatively flat as the width of distribution increases. The corresponding relative amplitude changes from 14% for a 0.1 μm distribution width to $\sim$2% for a 1.7 μm distribution width. In contrast, the forward scattering spectra do not show a strong dependence on the width for narrow distributions but undergo significant changes as the width of distribution becomes larger than 0.5 μm. The relative amplitude of the forward component varies from 40% for the narrowest distribution to 13% for the widest one.

The forward scattering spectra show prominent changes as the relative refractive index of scatterers increases from 1.03 to 1.048 [Figure 6(e)]. Corresponding changes in the relative amplitudes are from 49% to 9%. Note that the alterations observed are very similar to those present as the mean scatterer diameter is increased [cf. Figures 6(a) and 5(e)]. To facilitate analysis of the dependence of the backward scattering spectra on the relative refractive index of scatterers, the calculated backscattering spectra were normalized to the same value at 570 nm [Figure 6(f)]. The backward component undergoes noticeable changes in the wavelength region between 420 and 540 nm; as the relative refractive index increases, the valley around 470 nm becomes more prominent. However, the relative amplitude of the alterations is just 1.7% for the relative index of $n_{\mathrm{rel}}=1.048$ and $\sim$1.2% for the more biologically relevant value of $n_{\mathrm{rel}}=1.037$.

The effect of the collection/illumination fiber NA on the forward and backward scattering components was also studied. We performed numerical simulations with a typical distribution of nuclear sizes with mean diameter of 6 μm and distribution width of 0.5 μm and NA's ranging from 0.22 to 0.4. It was shown that, while the amplitudes of the forward and backward scattering components increase as the NA of the illumination/collection fibers increases, the shapes of the curves do not undergo any significant changes for the simulated NAs. Therefore, we used the most common fibers with a NA of 0.22 in our probe design.

To reduce the number of fitting parameters in analysis of polarized reflectance spectra of epithelium *in vivo* we used epithelial cells from the oral cavity to determine the relative refractive index of these nuclei. The polarized reflectance spectra of cells were measured in a highly concentrated solution of BSA to match the refractive index of cytoplasm described in Refs. 6 and 19. The mean diameter and standard deviation of sizes of nuclei were determined by light microscopy ($d=11\pm1$ μm). The depolarization ratio spectrum obtained for the cells was fit to a linear combination of forward and backward scattering Mie components plus a constant dc offset using the refractive index of nuclei as a fitting parameter to achieve the best fit. The fitting procedure yielded a refractive index of the nuclei of $n_{\mathrm{nucl}}=1.42351\pm0.0007$, which corresponds to the relative refractive index of $n_{\mathrm{rel}}=1.036$.

In vivo measurements of the oral cavity mucosa obtained using the polarization sensitive fiber probe are shown in Figure 7. Strong hemoglobin absorption is evident in the unprocessed reflectance spectra [Figures 7(a) and 7(c)]. Both the hemoglobin absorption and the diffuse background are dramatically reduced when the perpendicular component of scattered light is subtracted from the parallel one. The resulting depolarization ratio spectra were described using Mie theory calculations with fixed refractive indices derived from the experiments with cells (refractive index of medium $n_{\mathrm{med}}=1.374\pm0.001$, refractive index of nuclei $n_{\mathrm{nucl}}=1.4235\pm0.0007$). The average diameter of nuclei retrieved from the

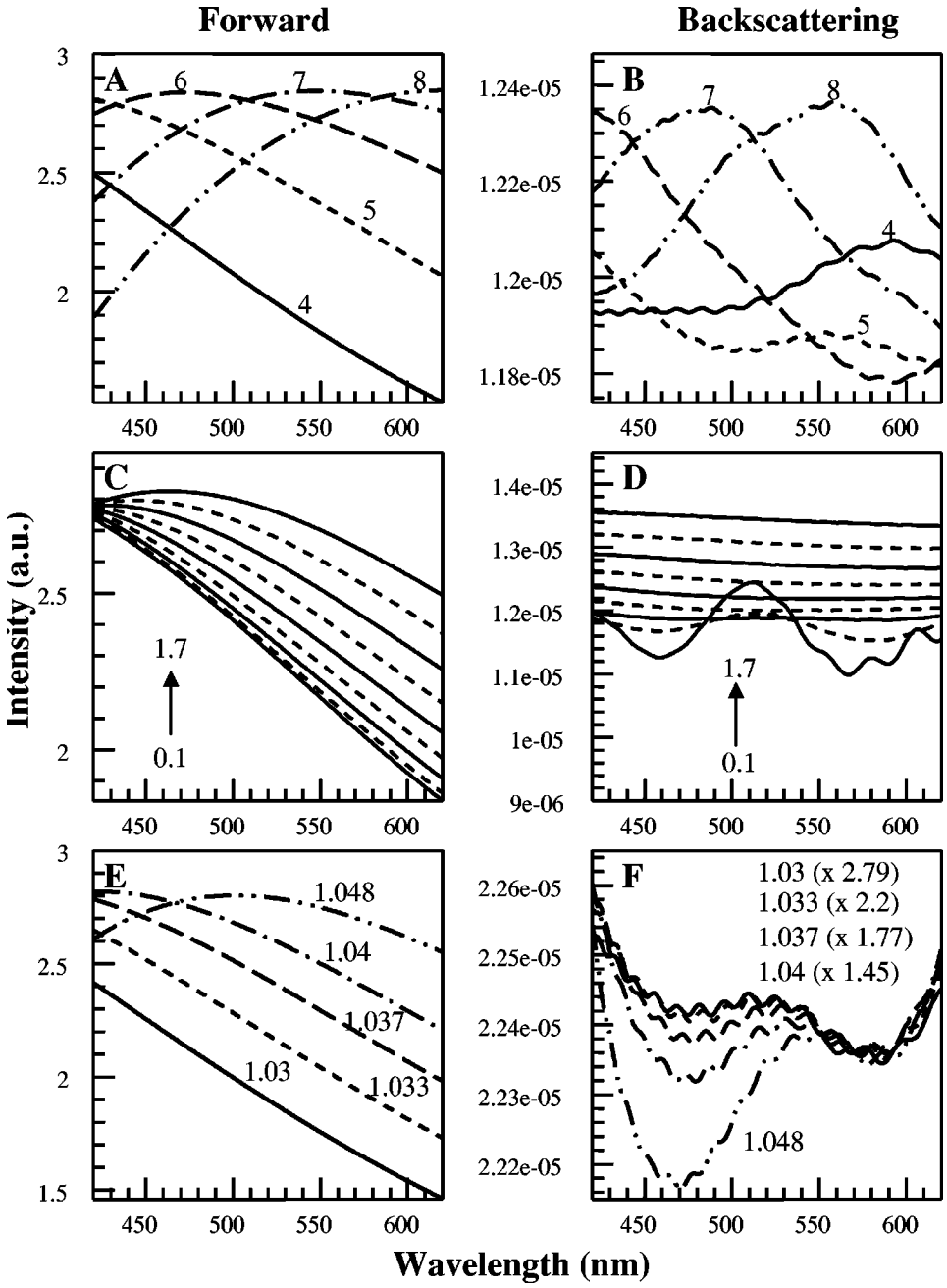

Fig. 6 Mie theory calculations for forward and backward scattering components of spherical scatterers for illumination/collection geometry of the fiber optic probe. The mean diameter, size distribution, and relative refractive index of the scatterers were varied over ranges characteristic of epithelial nuclei. Calculations for mean diameters were made with fixed relative refractive index $n_{rel}=1.036$ and size distribution $\Delta d=0.5$ μm. (a) Forward and (b) backward scattering components for mean diameters of 4 (solid curve), 5 (short dashed curve), 6 (long dashed curve), 7 (dot-dashed curve), and 8 μm (dot-dot-dashed curve). Mie calculations of (c) forward and (d) backscattering components associated with an increase in the size distribution of scatterers with fixed mean diameter $d=4.7$ μm and relative refractive index $n_{rel}=1.036$; the calculations are performed in 0.2 μm increments beginning at 0.1 μm; the arrows show the direction of the changes with an increase in size distribution. The curves in (c) and (d) are shown on the same relative scale. Mie calculations of (e) forward and (f) backward scattering components associated with an increase in the relative refractive index of scatterers with fixed mean diameter $d=4.7$ μm and size distribution of diameters $\Delta d=0.5$ μm: $n_{rel}=1.03$ (solid curve), 1.033 (short dashed curve), 1.037 (long dashed curve), 1.04 (dot-dashed curve), and 1.048 (dot-dot-dashed curve).

fits was 5.0 μm. Figures 7(b) and 7(d) show the fitting curves and the components used to describe the experimental depolarization ratio curves.

6 Discussion and Conclusions

Recently, we[6] and others[7–9] have demonstrated that polarized reflectance spectroscopy can be used to selectively detect the size-dependant scattering signatures of epithelial cells in the presence of both a strong diffusely scattering background and hemoglobin absorption. This opens up an exciting opportunity to develop noninvasive optical devices that can provide in real time diagnostically useful quantitative information about tissue morphology. Since nuclear morphology is a key param-

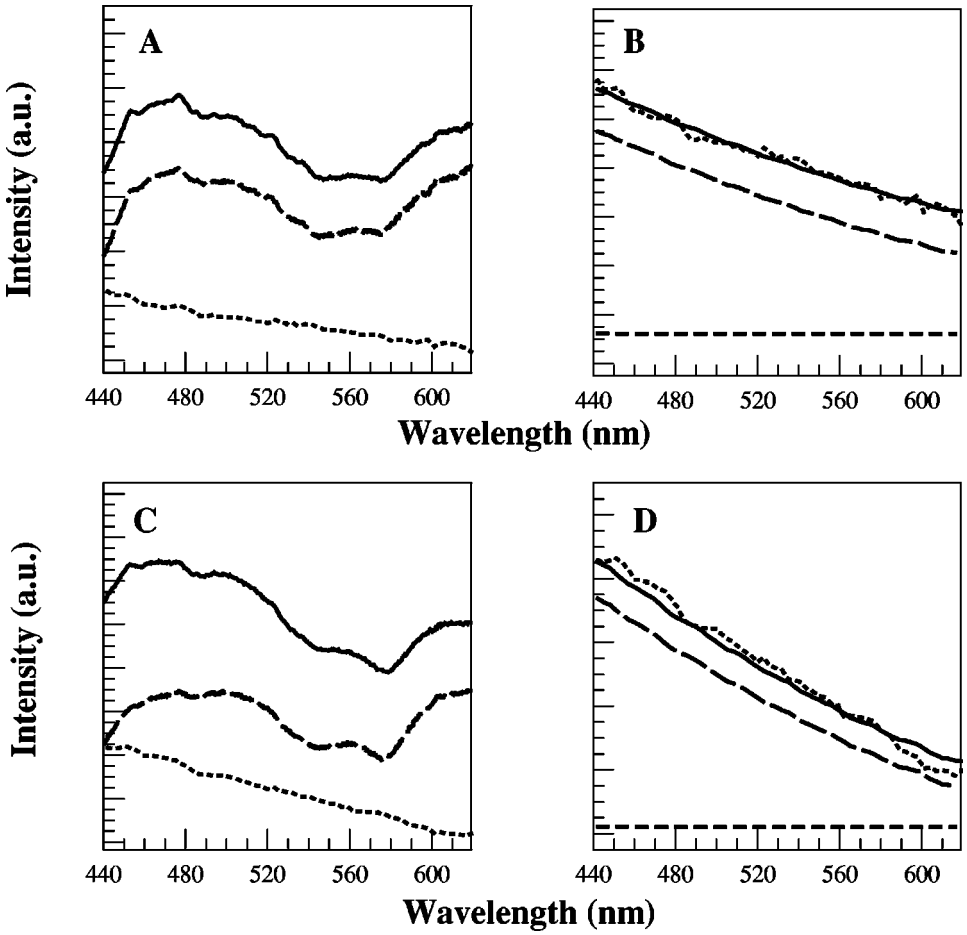

Fig. 7 Oral cavity reflectance spectra obtained *in vivo* for two different volunteers using the fiber optic probe and corresponding fits [(a) and (b) correspond to the volunteer 1, (c) and (d) correspond to the volunteer 2]. (a), (c) Reflectance spectra obtained using parallel collection fiber (solid curve), perpendicular collection fiber (long dashed curve), and the depolarization ratio spectrum (dotted curve). (b), (d) Depolarization ratio (dotted curve), calculated fit (solid curve), forward scattering component (long dashed curve), backward scattering component (short dashed curve).

eter in the diagnosis of cancers and pre-cancers, polarized reflectance spectroscopy could be used as a new modality to improve early detection of pre-cancers *in vivo*. Here, we demonstrated a fiber optic probe which can be used to measure polarized reflectance spectra *in vivo*. First, we showed that depolarization ratio spectra obtained using this fiber probe can be described as a linear combination of forward and backscattering spectra of the scatterers for polystyrene spheres placed atop a strongly diffusely scattering substrate. Then we performed Mie theory calculations to analyze the morphological parameters of epithelial tissue that most strongly influence polarized reflectance measurements with the fiber probe. Finally, we applied the fiber probe setup to assess the morphology of normal oral cavity mucosa *in vivo*.

Figure 5 showed that a linear combination of forward and backward scattering components is needed to fully describe the depolarization ratio spectrum obtained for polystyrene beads in water. The polystyrene beads, with well-known diameter and refractive index, provide a well-characterized phantom to verify the theoretical model that describes depolarization ratio spectra obtained using the fiber probe. The data presented are very similar to those reported in Ref. 6 and they support our conclusion that the approaches previously developed by us to analyze spectra obtained using a benchtop polarized reflectance spectrometer can be directly transferred to the probe geometry.

To make a transition from polarized reflectance measurements of well-characterized phantoms to *in vivo* epithelial human tissue it is important to understand how forward and backscattering components of tissue scattering are related to tissue morphology. Our primary interest was to retrieve the main morphological signatures associated with cancer development which are increased nuclear size, increased nuclear/cytoplasmic ratio, increased width of the nuclear size distribution, and hyperchromasia. To determine the feasibility of measuring these parameters via this spectroscopic approach we performed Mie theory calculations that approximated nuclei as spherical scatterers with a characteristic average refractive index.

First, we fixed the refractive index using the value determined in experiments with oral epithelial cells in suspension and varied the mean diameter and distribution of sizes of nuclei. Our calculations showed a strong dependence of both the forward and the backward scattering components on the mean nuclear diameter [Figures 6(a) and 6(b)]. However, the relative amplitude of the forward component is at least an order

of magnitude higher than that of the backscattering one. Therefore, backscattering spectra appear flat compared to forward scattering spectra. Thus, the forward scattering component is the decisive factor which determines the mean diameter of scatterers from polarization reflectance measurements. The backward component will play a decisive role only when its contribution to depolarization ratio spectra is bigger than the contribution of the forward component [coefficient b in Eq. (2)] by a factor of $\sim 10^6$. In the case of different widths of size distributions, the backscattering and forward scattering components appear to be complementary, since backscattering shows high sensitivity to size distributions with widths less than ~ 0.5 μm and the forward scattering is more sensitive to size distributions with widths larger than 0.5 μm [Figures 6(c) and 6(d)]. These results show promise that the combination of forward and backward scattering components can be used to retrieve both the mean diameter and distribution width of nuclei *in vivo*.

Consequently, we fixed the mean diameter and size distribution of scatterers and changed the relative refractive index from 1.03 to 1.048. Changes in refractive index cause similar alterations in the forward scattering component as changes of the mean diameter of scatterers [cf. (a) and (e) in Figure 6]. Therefore, it can be problematic to separate contributions of these two parameters in the forward scattering of nuclei. In the case of the backward component the average amplitude of scattering significantly increases with and increase of the refractive index but the relative amplitude undergoes only minor alterations, $\sim 1.7\%$ ($n_{\mathrm{rel}} = 1.048$) or less [Figure 6(f)]. It is doubtful that these subtle changes of the backscattering component can be measured in the presence of the sharply changing forward component. Even in geometries in which a backscattering component can be measured separately it would require a setup with a signal-to-noise ratio significantly higher than 60 in order to be able to see the shape of the individual curves shown in Figure 6(f). The signal-to-noise ratio should be another ~ 10 times higher in order to detect alterations in the backscattering curves associated with changes in relative refractive index in the physiologically relevant range between 1.03 and 1.037. This requirement may create technical difficulties in implementation of polarized reflectance spectroscopy for *in vivo* measurements. Therefore, we believe that it is impractical to use the shape of the backscattering component to retrieve the relative refractive index of scatterers. However, some information about changes in the relative refractive index can be obtained from a comparison of the relative contribution of backward and forward components in experimental depolarization ratio spectra. Our Mie theory calculations showed that the average intensity of the forward component does not strongly depend on changes in the relative refractive index [Figure 6(e)]. The intensity of the backscattering component in contrast strongly depends on the relative refractive index of scatterers. The average amplitude of the backscattering component varies approximately by 30% when the relative refractive index increases by 0.005. Therefore, changes in the relative contribution of forward and backscattering components could be indicative of variations in the relative refractive index of scatterers.

Our present analysis provides only a qualitative picture of alterations in forward and backward scattering of nuclei associated with changes in their main morphological parameters. More phantom experiments are needed to determine quantitatively the sensitivity of fiber based polarized reflectance spectroscopy to the morphology of nuclei. In future experiments, we plan to use phantoms of increased complexity to address this problem: suspensions of spheres with known mean diameter and width of distributions, well-characterized cell lines, and realistic three-dimensional tissue phantoms.[15]

Examples of *in vivo* measurements of oral cavity mucosa using the polarization sensitive fiber optic probe were shown in Figure 7. The use of polarization illumination/detection significantly reduces the contribution of hemoglobin absorption according to the spectra measured. However, it was found that in some cases residual blood absorption remained in the processed spectra, and this can make quantitative analysis difficult. We are currently optimizing the fiber probe to increase the portion of collected light scattered by epithelium and decrease the contribution of light scattered by stroma. This can be achieved by increasing the overlap between the illumination and collection cones in the epithelium and by suppressing the acceptance angle for light scattered by stroma.

In our current approach we used a suspension of epithelial cells in highly concentrated BSA solution to determine the relative refractive index of nuclei.[6] A high concentration of BSA allows one to match the refractive indices of the cellular cytoplasm and the surrounding medium.[19] This results in a dramatic decrease in scattering associated with cellular cytoplasm while the nuclear scattering remains the same. The refractive index obtained from experiments with cell suspensions is used as a fixed parameter in fitting polarized reflectance spectra of epithelial tissue. This approach allows us to avoid the uncertainty associated with simultaneous determination of the relative refractive index, mean diameter, and size distribution of nuclei *in vivo*.

The experimental *in vivo* depolarization ratio curves were fit using Mie theory calculations with the relative refractive index of nuclei $n_{\mathrm{rel}} = 1.036$. The best fits were achieved for mean nuclear diameters of $d_{\mathrm{nucl}} = 5.0$ μm. The mean diameter from morphometric measurements of normal oral epithelium of the cheek $d = 6.0$ μm was previously reported.[18] The mean diameter extracted from polarized reflectance measurements agrees reasonably well with previous measurements.

In summary, we have developed a fiber optic probe for an elastic polarization spectroscopy technique which allows one to dramatically decrease the contribution of both diffusely scattered light and hemoglobin absorption that originate from stroma. The performance of the fiber probe was tested using a suspension of polystyrene spheres placed atop a diffusely scattering substrate and *in vivo* measurements of oral cavity mucosa. Subsequent analysis of the spectra measured in terms of Mie theory revealed diagnostically useful morphological parameters of nuclei, which are currently available only through the painful procedure of excision biopsy. The fiber optic probe will allow measurements to be performed *in vivo* in clinical settings that will bridge the gap between benchtop studies and clinical applications of polarized reflectance spectroscopy.

Acknowledgments

The authors acknowledge the contribution of Dafna Lotan for preparation of specimens. They thank Dr. Reuben Lotan of the University of Texas M. D. Anderson Cancer Center for pro-

viding specimen cultures of cells. Financial support from the Whitaker Foundation is gratefully acknowledged.

References

1. R. T. Greenlee, M. B. Hill-Harmon, T. Murray, and M. Thun, ''Cancer Statistics, 2001,'' *Ca-Cancer J. Clin.* **51**, 15–36 (2001).
2. R. Cotran, V. Kumar, and S. Robbins, *Pathologic Basis of Disease*, 5th ed., Chap. 7, Saunders, Philadelphia (1994).
3. G. A. Wagnieres, W. M. Star, and B. C. Wilson, ''*In vivo* fluorescence spectroscopy and imaging for oncological applications,'' *Photochem. Photobiol.* **68**(5), 603–632 (1998).
4. R. Richards-Kortum and E. Sevick-Muraca, ''Quantitative optical spectroscopy for tissue diagnosis,'' *Annu. Rev. Chem.* **47**, 555–606 (1996).
5. N. Ramanujam, ''Fluorescence spectroscopy *in vivo*'' in *Encyclopedia of Analytical Chemistry*, R. A. Meyers, Ed., Vol. 1, pp. 20–56, Wiley, Chichester, UK (2000).
6. K. Sokolov, R. Drezek, K. Gossage, and R. Richards-Kortum, ''Reflectance spectroscopy with polarized light: Is it sensitive to cellular and nuclear morphology,'' *Opt. Express* **5**, 302–317 (1999).
7. L. T. Perelmanet al., ''Observation of periodic fine structure in reflectance from biological tissue: A new technique for measuring nuclear size distribution,'' *Phys. Rev. Lett.* **80**, 627–630 (1998).
8. V. Backman, R. Gurjar, K. Badizadegan, I. Itzkan, R. Dasari, L. T. Perelman, and M. S. Feld, ''Polarized light scattering spectroscopy for quantitative measurements of epithelial cellular structures *in situ*,'' *IEEE J. Sel. Top. Quantum Electron.* **5**, (1999).
9. T. M. Johnson and J. R. Mourant, ''Polarized wavelength-dependent measurements of turbid media,'' *Opt. Express* **4**, 200–216 (1999).
10. J. R. Mourant, T. Fuselier, J. Boyer, T. M. Johnson, and I. J. Bigio, ''Predictions and measurements of scattering and absorption over broad wavelength ranges in tissue phantoms,'' *Appl. Opt.* **36**, 949–57 (1997).
11. R. R. Anderson, ''Polarized light examination and photography of the skin,'' *Arch. Dermatol.* **127**, 1000–1005 (1991).
12. S. G. Desmos and R. R. Alfano, ''Optical polarization imaging,'' *Appl. Opt.* **36**, 150–155 (1998).
13. S. L. Jacques, J. Roman, and K. Lee, ''Imaging superficial tissues with polarized light,'' *Lasers Surg. Med.* **26**, 119–129 (2000).
14. I. J. Bigio and J. R. Mourant, ''Ultraviolet and visible spectroscopies for tissue diagnostics: Fluorescence spectroscopy and elastic-scattering spectroscopy,'' *Phys. Med. Biol.* **42**, 803–814 (1997).
15. K. Sokolov, J. Galvan, A. Myakov, A. Lacy, R. Lotan, and R. Richards-Kortum, ''Realistic three-dimensional epithelial tissue phantoms for biomedical optics,'' *J. Biomed. Opt.* **7**(1), 148–156 (2002).
16. J. Qu, S. MacAuluay, S. Lam, and B. Palcic, ''Laser-induced fluorescence spectroscopy at endoscopy: Tissue optics, Monte Carlo modeling, and *in vivo* measurements,'' *Opt. Eng.* **34**, 3334–3343 (1995).
17. H. van de Hulst, *Light Scattering by Small Particles*, Dover, New York (1957).
18. Y. Jin, F. H. White, and L. Yang, ''A histological morphometric study of nuclear size in benign and malignant neoplasm of the human cheek,'' *Histopathology* **23**, 271–274 (1993).
19. R. Barer, ''Refractometry and interferometry of living cells,'' *J. Opt. Soc. Am.* **47**, 545–556 (1957).